ADVANCED OPTICAL MATERIALS
www.advopticalmat.de

Enhanced Evanescent Field Coupling of Smart Particles in Tubular Optical Microcavity for Sensing Application

*Shuo Yang, Yunqi Wang, Ye Kong, Gaoshan Huang, Zhe Zhao, Yang Wang, Borui Xu, Jizhai Cui, and Yongfeng Mei**

Whispering-gallery mode (WGM) optical microcavity with enhanced evanescent field is one of the most perfect systems to study light–matter interaction. Unique sensing devices and potential applications with excellent performance can be expected by integrating smart particles into the microcavity, such as small mode volume and high sensitivity. Here, it is demonstrated that rolled-up tubular optical microcavity decorated with palladium (Pd) nanoparticles (NPs) is capable for hydrogen (H_2) sensing. Such microtube with subwavelength wall thickness exhibits enhanced sensing performance, e.g., detection limit of 1000 parts per million (ppm) and sensitivity in the order of 10^{-5} nm ppm^{-1}, due to strong coupling in the evanescent field. Experiments and simulations are compared and guided the optimization for high figures of merit. The approach proves a unique route to couple smart particles with rolled-up WGM microcavity for gas sensing, which have great application potentials in the field of nanophotonics and smart sensors.

1. Introduction

Optical microcavities, by virtue of their intrinsic safety of electromagnetic interference immunity and remote manipulation capability, have attracted great attention in research of environmental sensing.[1,2] Among them, whispering gallery mode (WGM) microcavities have been intensively investigated due to their high quality factors (Q factors) and small mode volumes (V_m).[3] In a WGM microcavity, light energy is confined by total internal reflection. From the microcavity, the evanescent field penetrates into the surrounding environment and interacts with ambient media. The phenomenon variations can be expressed as changes in optical signal, such as resonant mode shift, mode splitting, and mode broadening. On the basis of light–matter interaction through evanescent field, various WGM microcavities include microspheres,[4–6] microdisks,[7–9] microrings,[10] microroids,[11] and microtubes[12–16] have been applied in humidity detection,[17–19] optofluidic detection,[20–24] nanoparticle detection,[25–27] and single cell detection.[5,28–32] As nanoparticles on microcavity surface can alter the electric field distribution and the optical characteristics of the microcavity, WGM microcavity with strong evanescent field can achieve effective nanoparticle detection with ultrahigh spatial resolution of 10 nm. Such characteristics have great significance in human diseases diagnose and environmental monitoring.[33,34] By integrating smart particles that can respond to external stimuli with microcavities, various optical microcavity-based sensing devices can be obtained by utilizing strong light–matter interaction via evanescent field coupling.

Palladium (Pd) is a favored hydrogen (H_2) stimuli-responsive material for its high sensitivity, selectivity, and reversible Pd-to-PdH_x (where x is the atomic ratio of H:Pd) phase transition characteristics.[35] The H_2 absorption process of Pd associates with volume change as well as many other physical properties changes, such as the change of refractive index and dielectric constant.[36,37] Previous investigation has demonstrated that the increase of H_2 concentration causes decrease of the real part and increase of the imaginary part of the complex refractive index of PdH_x.[38] The property changes then induce optical signal variations through evanescent field coupling.[39–40] Here, we proposed and designed a unique coupling system with smart nanoparticles and tubular microcavity in both theoretical simulation and experimental demonstration. Smart Pd nanoparticles (NPs), which are mechanically stable and alleviate the destruction caused by phase transition[41–42] were integrated to tubular WGM microcavity with enhanced evanescent field by nanomembrane rolled-up technology for H_2 sensing.[43–45] As H_2 concentration increases, the rolled-up microcavity with Pd NPs decoration exhibits a resonant peak shift with good repeatability and

S. Yang, Y. Q. Wang, Y. Kong, G. S. Huang, Z. Zhao, Y. Wang, B. R. Xu, J. Z. Cui, Y. F. Mei
Department of Materials Science
Fudan University
Shanghai 200433, P. R. China
E-mail: yfm@fudan.edu.cn

S. Yang, Y. Q. Wang, Y. Kong, G. S. Huang, Z. Zhao, Y. Wang, J. Z. Cui, Y. F. Mei
International Institute for Intelligent Nanorobots and Nanosystems
Fudan University
Shanghai 200438, P. R. China

B. R. Xu, Y. F. Mei
Shanghai Frontiers Science Research Base of Intelligent Optoelectronics and Perception
Institute of Optoelectronics
Fudan University
Shanghai 200433, P. R. China

G. S. Huang, B. R. Xu, J. Z. Cui, Y. F. Mei
Yiwu Research Institute of Fudan University
Yiwu, Zhejiang 322000, P. R. China

The ORCID identification number(s) for the author(s) of this article can be found under https://doi.org/10.1002/adom.202102158.

DOI: 10.1002/adom.202102158

selectivity. Sensitivity of ≈10^{-5} nm ppm^{-1} and detection limit of ≈1000 ppm were achieved. We have also investigated the highest figures of merit at a suitable tube wall thickness via both experimental and theoretical studies. This work proves that smart material-decorated microcavity with modulated wall thickness is promising in realizing highly sensitive gas sensor.

2. Results and Discussion

To investigate the enhanced evanescent field of microcavities, simulations were adopted to identify the relationship between the wall thickness and optical characteristics, and the results are shown in **Figure 1**. Figure 1a–c shows schematic diagrams, electric intensity profiles, and radial electric intensity distributions from left to right of WGM microcavities with different geometries, respectively. In schematic diagrams, single 100 nm radius Pd NPs are attached to microcavities with the same radius of 10.65 μm, but with different wall thicknesses of 10.65 μm (microdisk), 650 nm (thick-wall microtube), and 80 nm (thin-wall microtube). Here, individual Pd NPs are introduced to study the intensity change of corresponding evanescent field. In electric intensity profiles, Pd NP is immersed in enhanced evanescent field, especially in ultrathin microtube wall with thickness of 80 nm in Figure 1c. However, in the radial electric intensity distributions, microcavity with thinner wall presents a weaker light confinement ability. Obviously, more light energy should leak out from the microcavity wall which is depicted as the yellow part. To further study the influence of wall thickness on optical properties, Q factors and external electric field intensity ratios (i.e., ratio between electric field intensity outside microcavity wall and total intensity) of microcavities with different wall thickness at resonant wavelength of ≈650 nm were calculated, and the results are shown in Figure 1d. Insets therein are schematic diagrams demonstrating the increase of tube wall thickness from a smaller value to a value closer to the radius. Q factor and external electric field ratio varies with wall thickness. Specifically, in thin-wall microtubes with wall thickness less than ≈100 nm (green part), Q factor enhances rapidly and external electric field ratio decreases rapidly as wall thickness increases. When wall thickness is above ≈1 μm, both Q factor and external electric field intensity ratio become stable. Because thicker-wall microcavities possess stronger capability of light confinement, leading to higher Q factor and weaker evanescent field intensity. For light confined in wall with a critical value, further increase of the wall thickness leads to neglectable influence on optical properties. It is worth noting that Q factor influences the resolution, and evanescent field determines the sensitivity in environmental sensing. Therefore, thin-wall microtube with a balanced Q factor and evanescent field intensity is of great importance for environmental sensing. By decorating the wall with different stimuli-response smart materials, the microcavities have demonstrated high sensitivity for molecule detection,[27] gas detection,[5] and optofluidic detection.[24] In this work, we demonstrate H_2 sensing as an example by integrating smart Pd NPs with thin-wall rolled-up high refractive index Y_2O_3/ZrO_2 tubular microcavity with enhanced evanescent field.

The proposed smart Pd NPs decorated rolled-up microtubes with H_2 sensing capability are depicted in **Figure 2**. Figure 2a is the diagram of the structure. Electric field profile of smart Pd NPs decorated microtube with average wall thickness of 80 nm (see the Supporting Information for details) and diameter of 20 μm is illustrated in Figure 2b, and the inset is a magnified image demonstrating Pd NP with diameter of ≈200 nm being immersed in evanescent field. Scanning electron microscopy (SEM) image of rolled-up Y_2O_3/ZrO_2 microtube array with diameter ≈20 μm is displayed in Figure 2c. Figure 2d shows the magnified SEM image of a single Y_2O_3/ZrO_2 microtube with clean smooth surface. Optical spectra of bare Y_2O_3/ZrO_2 microtubes placed in air and 4% H_2 are shown in Figure 2e. Apparently, the resonant peaks remain nearly the same, which indicates that bare Y_2O_3/ZrO_2 microcavities are incapable for H_2 sensing. Then, Pd NPs were blown onto the microtube through a plastic nozzle via a pump with a flow rate of ≈100 standard cubic centimeters per minute. Figure 2f (middle) and Figure 2g (edge) show the morphologies of the sample after smart Pd NPs decoration. One can see that Pd NPs with an average diameter of ≈200 nm were uniformly distributed on the surface of microtubes (see details in Figures S1–S4 of the Supporting Information), and this leads to significant weakening of the mode (Figure S5, Supporting Information). Figure 2h shows corresponding optical spectra of smart Pd NPs-decorated Y_2O_3/ZrO_2 microtubes placed in air and 4% H_2. As the red dashed line indicates, a blue shift of ≈0.3 nm is observed after the sample was immersed in 4% H_2. This blue shift is ascribed to the refractive index decrease due to Pd-to-PdH_x transition.[46] Following the WGM resonant condition in microtubes by Equation (1)[47]

$$2\pi Rn_{\text{eff}} = m\lambda \tag{1}$$

where R is the average radius of the microtube, λ is the resonant wavelength, n_{eff} is the effective refractive index of the microtube (see details in Figure S6 of the Supporting Information), and m is the azimuthal number, when Pd NPs react with H_2 molecules, the Pd-to-PdH_x transition causes reduced refractive index, and correspondingly, the decrease of n_{eff} leads to blue shift of resonant wavelength λ for the same azimuthal mode.[48–49]

H_2 sensing performance was investigated in detail by using schematical experimental setup shown in **Figure 3**a. H_2 concentration in gas chamber is controlled by regulating the flow rate of 4% H_2 and pure N_2 via flow controllers. The optical spectra are recorded and analyzed. Figure 3b shows measured optical spectra of a smart Pd NPs-decorated Y_2O_3/ZrO_2 microtube in atmospheres with H_2 gas of different concentrations. The resonant peaks shift to shorter wavelength with the increase of H_2 concentration, as the Pd-to-PdH_x transition decreases the refractive index (see details in Figures S7 and S8 of the Supporting Information). After removing H_2, resonant peaks recover to the initial position because of the reversible Pd-to-PdH_x transition. It is worth noting that the resonant peak shifts linearly with the increase of H_2 concentrations, and this is demonstrated by the linear fitting in Figure 3c.

Sensitivity (S) is an important parameter of sensor and is determined by[50]

$$S = \frac{\Delta\lambda}{\Delta c} \tag{2}$$

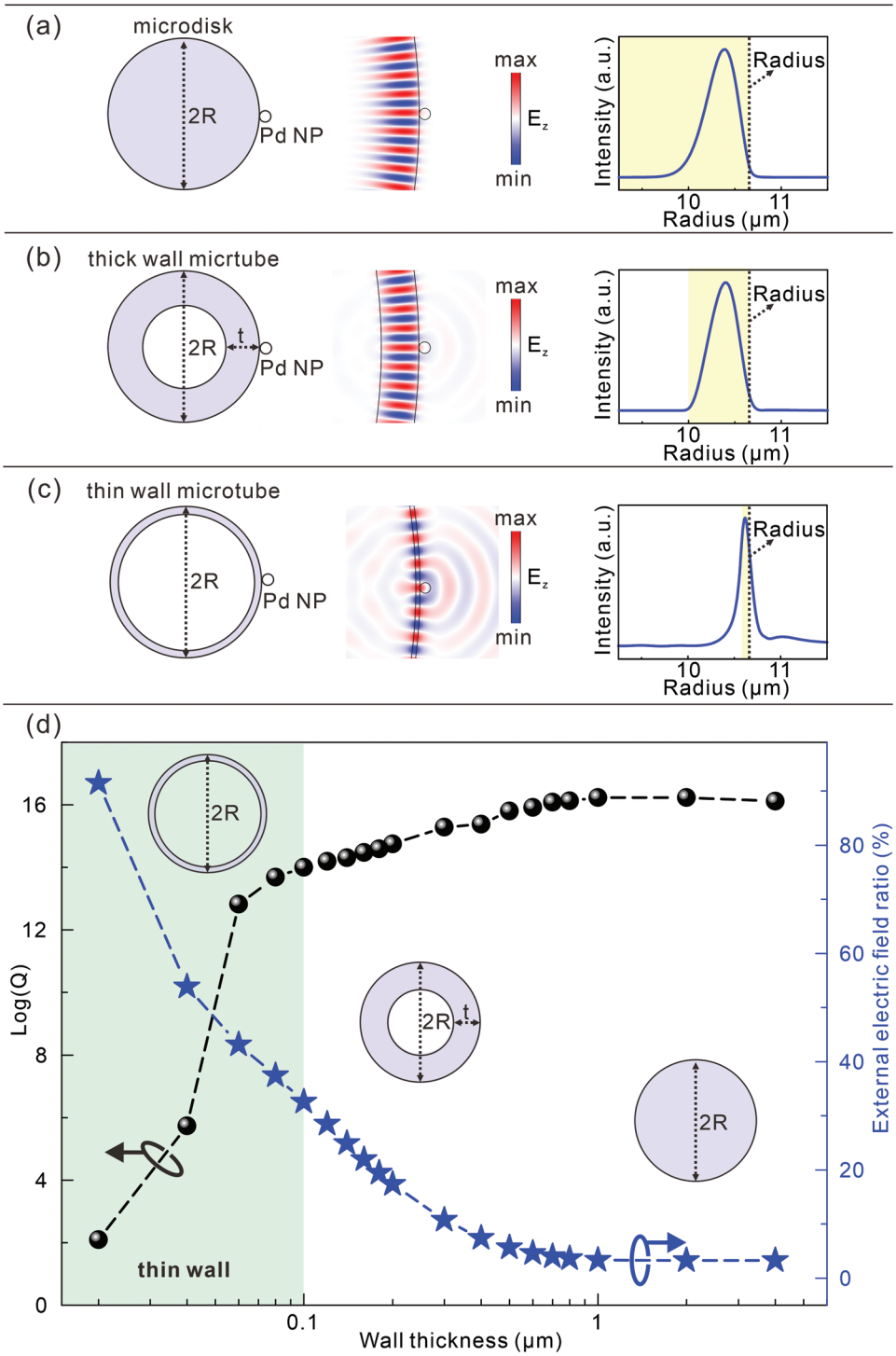

Figure 1. a–c) Schematic diagrams of microdisk, thick-wall microtube, thin-wall microtube with their corresponding electric field profile and radial distribution of electric intensity. In the electric field profile, the black circle represents Pd NP on the microcavity surface. In radial distribution of electric intensity, the gray dashed lines indicate the microcavity radius and the yellow part represents the microcavity wall. d) Calculated external electric field ratio and *Q* factor as a function of wall thickness. With increasement of wall thickness, microcavity changes from a thin-wall microtube to a thick-wall microtube and then to a microdisk. The green part shows thin-wall microtubes with wall thickness less than 100 nm.

where $\Delta\lambda$ is the resonant peak shift of the same azimuthal number and Δc is the corresponding change of H_2 concentration. Here, a sensitivity in the order of 10^{-5} nm ppm^{-1} can be calculated by using the average resonant peak shift of ≈1 nm, as shown in Figure 3d. Detection limit (DL) is another important parameter for sensor and can be calculated by[51]

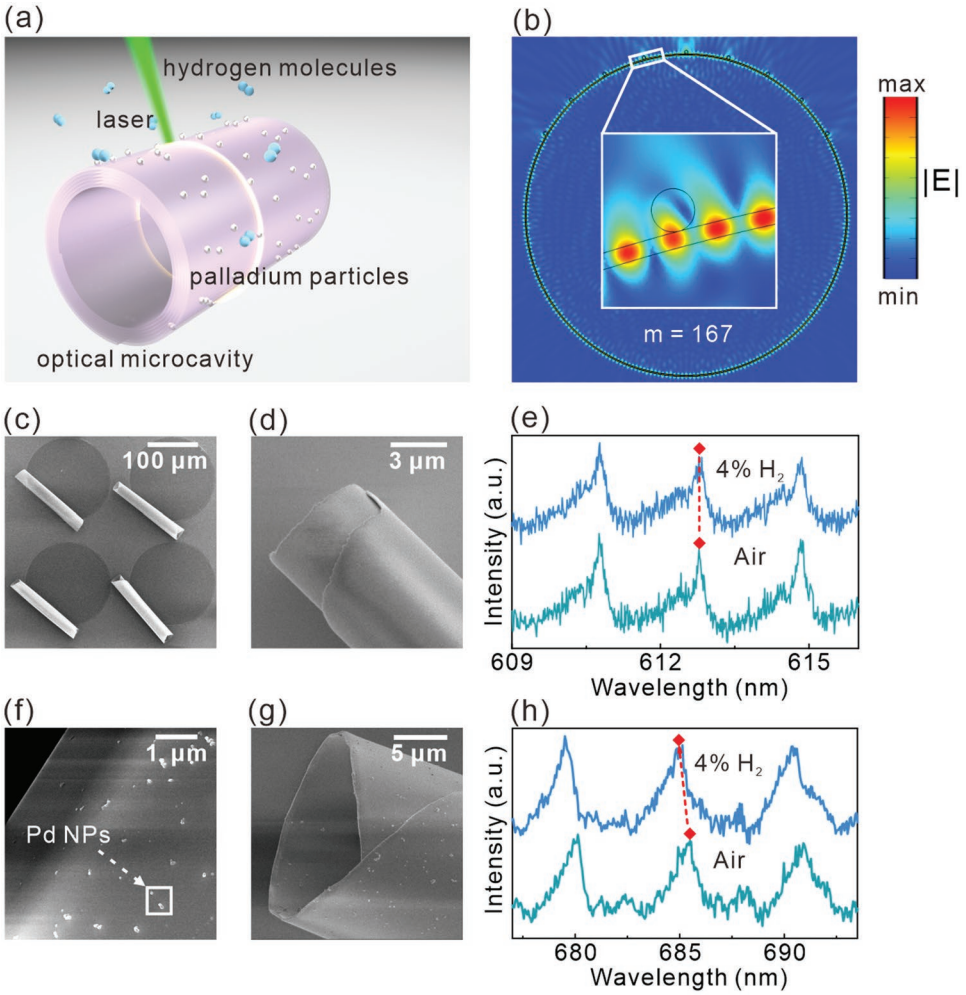

Figure 2. a) Schematic diagram of a smart Pd NPs-decorated optical microcavity being excited by a laser beam. b) Calculated electric field profile of mode with azimuthal number $m = 167$ in smart Pd NPs-decorated microtube with a diameter of 20 μm. c) SEM image of a rolled-up Y_2O_3/ZrO_2 microtube array. d) Magnified SEM image of a microtube. e) Measured optical spectra of a bare Y_2O_3/ZrO_2 microtube placed in air and 4% H_2. The red squares mark the resonant peak position, which are crossed by the vertical red dashed line. f) SEM image of middle part of a smart Pd NPs-decorated Y_2O_3/ZrO_2 microtube. g) SEM image of edge part of a smart Pd NPs-decorated Y_2O_3/ZrO_2 microtube. h) Measured optical resonant spectra of a smart Pd NPs-decorated Y_2O_3/ZrO_2 microtube placed in air and 4% H_2. The red squares mark the resonant peak position and the red dashed line demonstrates the shift of resonant peaks.

$$DL = 3\sigma / S \tag{3}$$

where σ is the standard deviation of the system noise/spectral resolution and is commonly determined by 1/50 of the full width at half maximum (FWHM) of the resonant peak. According to our experiment, the line width is ≈1 nm. Thus, the obtained detection limit of smart Pd NPs-decorated microcavities is in the order of 1000 ppm.

Repeatability is also an important parameter for sensing device. We measured the repeatability of the smart Pd NPs-decorated microtube with fixed experimental conditions shown in **Figure 4**a. First, optical spectrum was measured in air. Then, 4% H_2 was introduced into the gas chamber and spectrum was measured. Compared with air, resonant peaks shift to shorter wavelength of ≈0.5 nm in 4% H_2. Then, H_2 in gas chamber was replaced by N_2 and resonant peaks recover to initial positions. We experimentally found that the response time towards 4% H_2 is ≈30 s and the recovery time is less than 2 min. The cycle of measurement was repeated for several times to confirm the repeatability of smart Pd NPs-decorated microtube for H_2 sensing. In order to measure the selectivity of the device, different gases were filled into the chamber. Optical spectra measured for smart Pd NPs-decorated microtube in air, 100% N_2, 100% CO_2, and 4% H_2 are shown in Figure 4b. Resonant peaks in air, 100% N_2 and 100% CO_2 are almost the same, while resonant peak in 4% H_2 shifts obviously, although minor uncertainty (<0.015 nm) can be observed due to uncompleted H_2 desorption. Figure 4c shows the absolute value of resonant peaks shift, which demonstrates that the smart Pd NPs-decorated microtubes are highly selective for H_2 detection due to Pd-to-PdH_x transition.

To search the ideal wall thickness for higher figures of merit (QS, which is defined as the product of Q factor and sensitivity), we modulated the tube wall thickness through

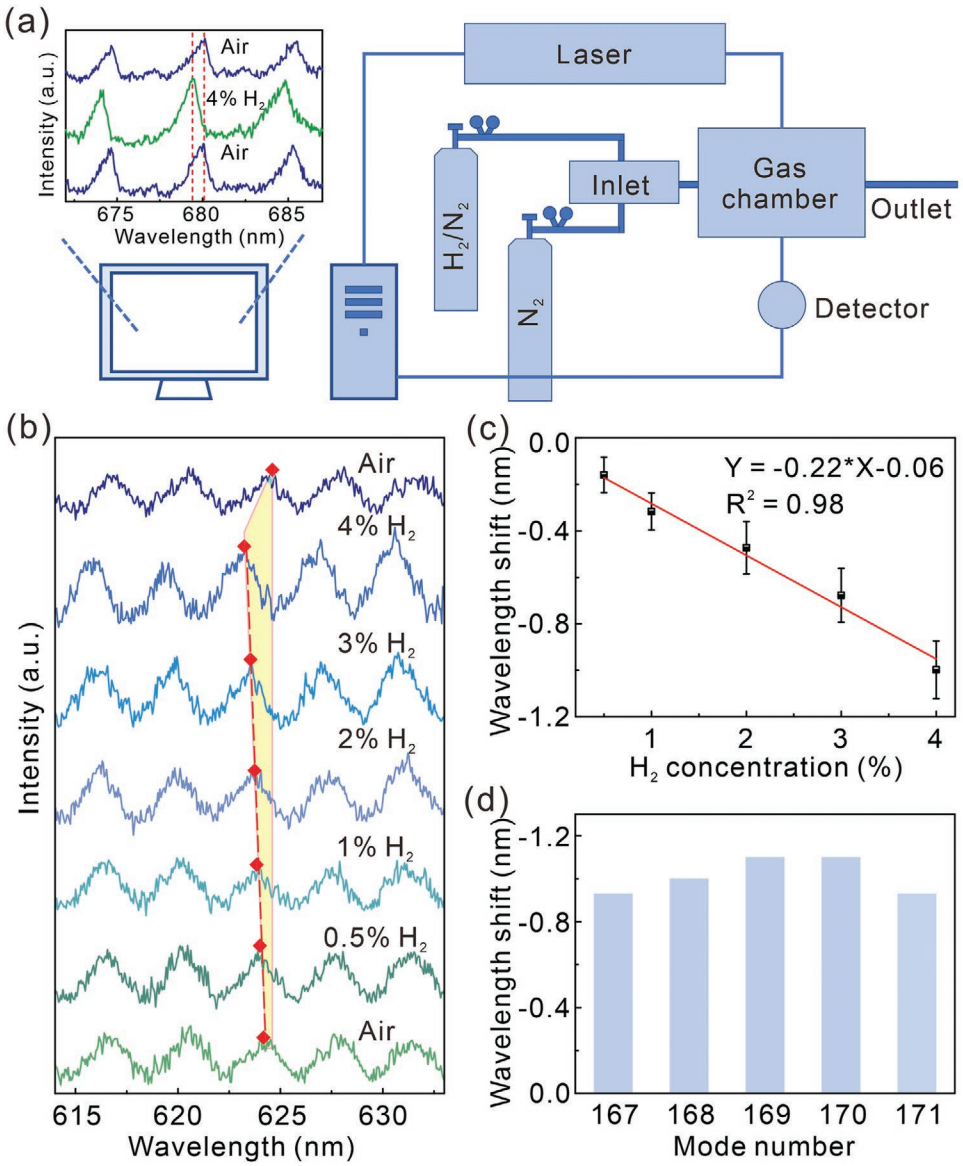

Figure 3. a) Schematic diagram of the experimental setup. Inset is a typical optical resonant spectra obtained from smart Pd NPs-decorated Y_2O_3/ZrO_2 microtube. The red dashed line indicates resonant peak shift when microtube was immersed in 4% H_2 and recover to initial position after removing H_2. b) Optical resonant spectra from the center of a ≈20 µm diameter tubular microcavity placed in atmospheres with various H_2 concentrations. The red squares mark the resonant peak position of mode $m = 169$. The red dashed line and yellow part refer to resonant wavelengths shift as function of H_2 concentration. c) Resonant peak shift for mode $m = 169$ in various H_2 concentrations compared with the mode measured in air. Red line is the linear fit with a residual sum of squares of ≈0.98. d) Resonant peaks shift in 4% H_2 compared with air for modes with $m = 167$–171.

experiments and simulations. **Figure 5**a,b is the electric field profile of Y_2O_3/ZrO_2 microtubes with wall thickness of 60 nm and 4000 nm, respectively. It is obvious that thinner wall exhibits stronger evanescent field. The relationship between wall thickness, *Q* factor, and sensitivity is studied by adjusting wall thickness by atomic layer deposition (ALD), a technique enables conformal coating from vapor phase.[52,53] Here, HfO_2 is chosen because of a similar refractive index to Y_2O_3/ZrO_2, and insets in Figure 5c and Figure S9 (Supporting Information) show optical images of microtubes coated by HfO_2 with different ALD cycles. Microtube in the left inset was coated with 10 nm HfO_2 on the inside and outside surfaces, and the total wall thickness is ≈60 nm. Microtube in the right was coated with 30 nm HfO_2 on the inside and outside surfaces, and the total wall thickness is ≈100 nm. With increase of wall thickness, *Q* factor (red star in Figure 5c) of the thin-wall microtubes increases gradually, while the corresponding sensitivity (black sphere in Figure 5c) decreases. On the other hand, thin-wall microtube also induces stronger evanescent field for Pd NPs, which leads to higher sensitivity.[54] However, enhanced light loss leads to a lower *Q* factor, causing deterioration of detection

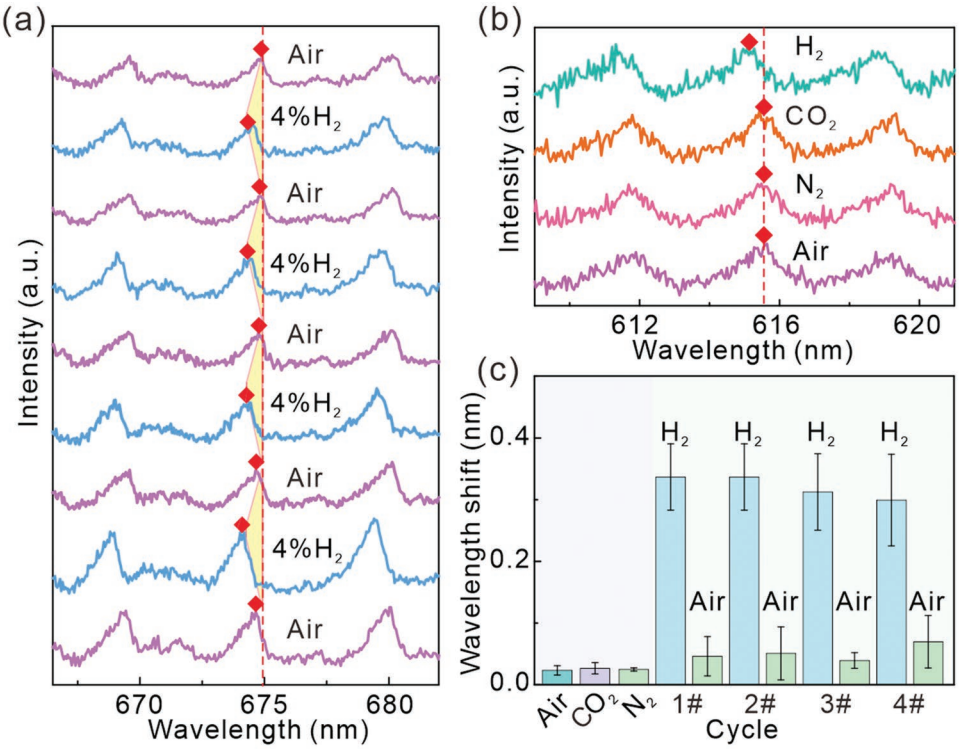

Figure 4. a) Measured optical resonant spectra from the center of a smart Pd NPs-decorated microtube with a diameter of ≈16 µm. The red squares mark the resonant peak positions of mode with azimuthal number $m = 125$. The red dashed line and yellow part refer to resonant peak shift. 4% H_2 and 100% N_2 are alternatively introduced for several cycles. b) Measured optical resonant spectra of Pd NPs-decorated microtube in air, 100% N_2, 100% CO_2, and 4% H_2. c) Resonant peak shift in different gases, demonstrating excellent selectivity.

limit due to large FWHM. Thus, seeking the balance between Q factor and sensitivity is of great importance for environmental sensing applications.[55] In order to improve the QS for H_2 sensing, QS, as a function of wall thickness, was studied both experimentally and theoretically and the results are presented in Figure 5d. The simulated QS first increases then tends towards a steady value, because the optical properties become stable as wall thickness is above ≈100 nm and further increase of the wall thickness leads to negligible additional light confinement. However, in our experiment, the Q factor is remarkably lower compared to theoretical value due to light scattering/loss caused by imperfections like the surface roughness of the nanomembrane and the voids between the rollings.[56] These influencing factors cannot be eliminated even with additional ALD HfO_2 layer, which is indicated by a smaller Q factor increase in our experiment (with respect to simulated case). Therefore, after reaching the maximum at a wall thickness of ≈60 nm, the experimental QS decreases with increasing wall thickness as the sensitivity decreases significantly owing to the weakened evanescent field. As a result, deviation between experimental QS and simulated QS can be noticed in Figure 5d, and the deviation becomes more obvious in the case of thick wall. Our results suggest a crucial wall thickness should be considered when designing sensing device by combining tubular WGM microcavity and smart material.

3. Conclusion

Smart particles of stimuli-response materials coupled with enhanced evanescent field of optical microcavities are suitable for environmental sensing. Our work demonstrated the feasibility of introducing smart Pd NPs to WGM microcavity with sub-wavelength wall thickness and strong evanescent field for highly sensitive H_2 sensing, and the Pd-to-PdH_x phase transition with refractive index change induced a nearly linear shift of resonant wavelength. Such smart Pd NPs-decorated rolled-up optical microcavities with sensitivity up to 10^{-5} nm ppm^{-1} and detection limit of 1000 ppm possess good selectivity and repeatability, and the highest QS was achieved at a crucial wall thickness. Our method offers a solution to couple smart particles in optical microcavities for nondestructive high-performance environmental sensing.

4. Experimental Section

Fabrication of Tubular Microcavity: First, an ARP-3510T photoresist (Allresist GmBH) sacrificial layer with thickness of ≈2 µm was uniformly spin-coated on the silicon substrate. The parameters are 600 rpm for 9 s followed by 4000 rpm for 30 s. Then, the samples were baked on a hot plate at 100 °C for 1 min. Mask aligner (MA6) was used to pattern photoresist into designed circles with various diameters via UV photolithography. Afterward, a 10 nm Y_2O_3 layer and a 40 nm ZrO_2 layer were sequentially deposited at deposition rate of 5 and 0.5 Å s^{-1}, respectively, by e-beam deposition (TSV70, Tenstar) with a glancing angle of 30°, which could

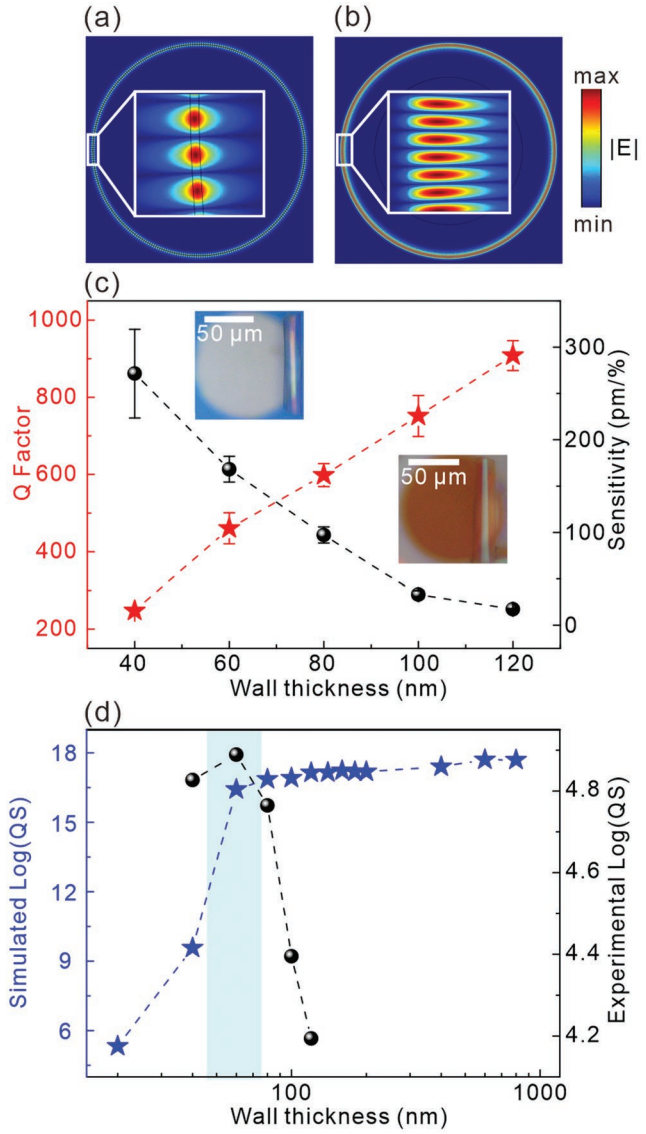

Figure 5. Electric field profile of a) thin-wall microtube with wall thickness of 60 nm and b) thick-wall microtube with wall thickness of 4000 nm. c) Experimental *Q* factor and sensitivity as a function of microtube wall thickness. The left inset is optical image of a rolled-up microtube with wall thickness of 60 nm. The right inset is optical image of a rolled-up microtube with wall thickness of 100 nm. d) Experimental and calculated QS as a function of microtube wall thickness. The blue part refers to the region corresponding to high QS in the experiment.

provide an etching window and bounding edge for microtubes attached on substate after release. The chamber temperature of e-beam deposition is 25 °C, and the base pressure is in the order of 10^{-4} Pa. After e-beam deposition, samples were immersed in acetone to selectively remove the photoresist layer, releasing Y_2O_3/ZrO_2 bilayer nanomembranes, which were rolled up to form microtubular structure. Finally, samples were dried in critical point dryer (CPD, Tousimis Autosamdri-815B) with liquid CO_2 as an intermedia to avoid collapse of microstructure due to surface tension of liquid in drying process. The diameter of microtube could be tuned by adjusting deposition parameters such as the nanomembranes thicknesses and the deposition rate.

ALD of HfO_2 Layer: HfO_2 coating layers of different thicknesses were prepared by ALD as a postprocessing to tune wall thickness of the microtubular structure. Besides, ALD HfO_2 layer could also mechanically strengthen the microcavities and improve the light confinement. In the ALD process, tetrakis(dimethylamino) hafnium (TDMAH) and DI water were used as precursors. A typical ALD cycle includes TDMAH pulse (150 ms), waiting time (30 s), N_2 purge (30 s), DI water pulse (20 ms), and waiting time (30 s).

Microstructural Characterizations: Morphological and compositional analyses of the samples were measured by field emission SEM equipped with energy dispersive spectrometer (Zeiss Sigma). The refractive index of Y_2O_3/ZrO_2 nanomembrane was measured by n&k 8000-CD multifunctional film analyzer (n&k Technology Inc.).

Simulation Model: Theoretical simulations were carried out based on the finite element method. In theoretical model, microtube with diameter of 20 μm was calculated with different wall thickness to study the influence of wall thickness on *Q* factor and sensitivity. The refractive index of Y_2O_3/ZrO_2 microtube is set to be 2.0, which is consistent with the experimental value of 1.93 (Figure S6, Supporting Information). The mesh size of the structure was designed to be smaller than 1/3 of the wavelength to ensure the quality of simulations.

Optical Sensing Test: The optical spectra were measured by Raman spectrometer (Horiba LabRAM HR Evolution) with an excitation wavelength of 532 nm. The laser power was set at 2.5 mW and the grating is 600 g mm^{-1}. The sample was placed in the chamber with quartz window, which is connected with gas flow controller.

Supporting Information

Supporting Information is available from the Wiley Online Library or from the author.

Acknowledgements

This work was supported by the National Key R&D Program of China (No. 2021YFE0191800), the Natural Science Foundation of China (Nos. 62005050, 51961145108, and 61975035), and the Science and Technology Commission of Shanghai Municipality (Nos. 19XD1400600 and 20501130700). Part of the experimental work had been carried out in Fudan Nanofabrication Laboratory.

Conflict of Interest

The authors declare no conflict of interest.

Data Availability Statement

The data that support the findings of this study are available from the corresponding author upon reasonable request.

Keywords

evanescent field, hydrogen sensors, palladium nanoparticles, rolled-up optical microcavities

Received: October 8, 2021
Revised: November 4, 2021
Published online: December 17, 2021

[1] K. J. Vahala, *Nature* **2003**, *424*, 839.
[2] Y. Y. Zhi, X. C. Yu, Q. H. Gong, L. Yang, Y. F. Xiao, *Adv. Mater.* **2017**, *29*, 1604920.

[3] X. Jiang, L. Shao, S.-X. Zhang, X. Yi, J. Wiersig, L. Wang, Q. Gong, M. Lončar, L. Yang, Y. Xiao, *Science* **2017**, *358*, 344.
[4] S. H. Huang, X. Jiang, B. Peng, C. Janisch, A. Cocking, Ş. K. Özdemir, Z. Liu, L. Yang, *Photonics Res.* **2018**, *6*, 346.
[5] A. K. Mallik, G. Farrell, M. Ramakrishnan, V. Kavungal, D. Liu, Q. Wu, Y. Semenova, *Opt. Express.* **2018**, *26*, 31829.
[6] Y. Liu, X. Jiang, C. Wang, L. Yang, *Appl. Phys. Lett.* **2020**, *116*, 201104.
[7] S. L. McCall, A. F. J. Levi, R. E. Slusher, S. J. Pearton, R. A. Logan, *Appl. Phys. Lett.* **1992**, *60*, 289.
[8] S.-K. Kim, S.-H. Kim, G.-H. Kim, H.-G. Park, D.-J. Shin, Y.-H. Lee, *Appl. Phys. Lett.* **2004**, *84*, 861.
[9] T. J. Kippenberg, J. Kalkman, A. Polman, K. J. Vahala, *Phys. Rev. A* **2006**, *74*, 051802.
[10] I. M. W. J. D. Suter, H. Zhu, X. Fan, *Appl. Opt.* **2007**, *46*, 389.
[11] J. C. Long, H. W. Chan, A. B. Churnside, E. A. Gulbis, M. C. Varney, J. C. Price, *Nature* **2003**, *421*, 922.
[12] Z. Tian, S. Li, S. Kiravittaya, B. Xu, S. Tang, H. Zhen, W. Lu, Y. Mei, *Nano Lett.* **2018**, *18*, 8035.
[13] J. Wang, Y. Yin, Q. Hao, S. Huang, E. Saei Ghareh Naz, O. G. Schmidt, L. Ma, *ACS Photonics* **2018**, *5*, 2060.
[14] S. Kiravittaya, V. A. Bolaños Quiñones, M. Benyoucef, A. Rastelli, O. G. Schmidt, *Appl. Phys. Lett.* **2009**, *94*, 141901.
[15] M. R. Foreman, J. D. Swaim, F. Vollmer, *Adv. Opt. Photonics* **2015**, *7*, 168.
[16] X. Jiang, A. J. Qavi, S. H. Huang, L. Yang, *Matter* **2020**, *3*, 371.
[17] S. Mehrabani, P. Kwong, M. Gupta, A. M. Armani, *Appl. Phys. Lett.* **2013**, *102*, 241101.
[18] J. Zhang, J. Zhong, Y. F. Fang, J. Wang, G. S. Huang, X. G. Cui, Y. F. Mei, *Nanoscale* **2014**, *6*, 13646.
[19] Y. Yin, J. Wang, X. Wang, S. Li, M. R. Jorgensen, J. Ren, S. Meng, L. Ma, O. G. Schmidt, *Sci. Adv.* **2019**, *5*, eaax6973.
[20] A. Bernardi, S. Kiravittaya, A. Rastelli, R. Songmuang, D. J. Thurmer, M. Benyoucef, O. G. Schmidt, *Appl. Phys. Lett.* **2008**, *93*, 094106.
[21] G. Huang, V. A. B. Quinones, F. Ding, S. Kiravittaya, Y. Mei, O. G. Schmidt, *ACS Nano* **2010**, *4*, 3123.
[22] V. A. Bolaños Quiñones, L. Ma, S. Li, M. Jorgensen, S. Kiravittaya, O. G. Schmidt, *Appl. Phys. Lett.* **2012**, *101*, 151107.
[23] Y. Li, Y. Fang, J. Wang, L. Wang, S. Tang, C. Jiang, L. Zheng, Y. Mei, *Lab Chip* **2016**, *16*, 4406.
[24] A. Madani, S. M. Harazim, V. A. Bolanos Quinones, M. Kleinert, A. Finn, E. S. Ghareh Naz, L. Ma, O. G. Schmidt, *Opt. Lett.* **2017**, *42*, 486.
[25] T. Lu, H. Lee, T. Chen, S. Herchak, J. H. Kim, S. E. Fraser, R. C. Flagan, K. Vahala, *Proc. Natl. Acad. Sci. USA* **2011**, *108*, 5976.
[26] J. D. Swaim, J. Knittel, W. P. Bowen, *Appl. Phys. Lett.* **2013**, *102*, 183106.
[27] Y. Zhi, X. C. Yu, Q. Gong, L. Yang, Y. F. Xiao, *Adv. Mater.* **2017**, *29*, 1604920.
[28] V. R. Dantham, S. Holler, C. Barbre, D. Keng, V. Kolchenko, S. Arnold, *Nano Lett.* **2013**, *13*, 3347.
[29] J. T. Kindt, M. S. Luchansky, A. J. Qavi, S. H. Lee, R. C. Bailey, *Anal. Chem.* **2013**, *85*, 10653.
[30] H. Ghali, H. Chibli, J. L. Nadeau, P. Bianucci, Y. A. Peter, *Biosensers* **2016**, *6*, 20.
[31] E. Gil-Santos, J. J. Ruz, O. Malvar, I. Favero, A. Lemaitre, P. M. Kosaka, S. Garcia-Lopez, M. Calleja, J. Tamayo, *Nat. Nanotechnol.* **2020**, *15*, 469.
[32] Z. Guo, Y. Qin, P. Chen, J. Hu, Y. Zhou, X. Zhao, Z. Liu, Y. Fei, X. Jiang, X. Wu, *Small* **2020**, *16*, 2000239.
[33] X. Yu, Y. Zhi, S. Tang, B. Li, Q. Gong, C. Qiu, Y. Xiao, *Light: Sci. Appl.* **2018**, *7*, 18003.
[34] B. Li, W. R. Clements, X. Yu, K. Shi, Q. Gong, Y. Xiao, *Proc. Natl. Acad. Sci. USA* **2014**, *111*, 14657.
[35] S. Dekura, H. Kobayashi, K. Kusada, H. Kitagawa, *ChemPhysChem* **2019**, *20*, 1158.
[36] P. S. Chauhan, S. Bhattacharya, *Int. J. Hydrogen Energy* **2019**, *44*, 26076.
[37] W. T. Koo, H. J. Cho, D. H. Kim, Y. H. Kim, H. Shin, R. M. Penner, I. D. Kim, *ACS Nano* **2020**, *14*, 14284.
[38] Y. S. Yi, D. C. Wu, P. Birar, Z. Yang, *IEEE Sens. J.* **2017**, *17*, 2042.
[39] M. Eryurek, Y. Karadag, N. Tasaltin, N. Kilinc, A. Kiraz, *Sens. Actuators, B* **2015**, *212*, 78.
[40] K. Cicek, M. Eryurek, A. Kiraz, *J. Opt. Soc. Am. B* **2017**, *34*, 1465.
[41] J. T. Yang, R. Fan, J. Li, F. L. Meng, *IEEE Sens. J.* **2019**, *19*, 6736.
[42] A. Baldi, T. C. Narayan, A. L. Koh, J. A. Dionne, *Nat. Mater.* **2014**, *13*, 1143.
[43] O. G. Schmidt, K. Eberl, *Nature* **2001**, *410*, 168.
[44] G. Huang, Y. Mei, *Adv. Mater.* **2012**, *24*, 2517.
[45] Z. Chen, G. Huang, I. Trase, X. Han, Y. Mei, *Phys. Rev. Appl.* **2016**, *5*, 017001.
[46] Y. Liu, N. Zhang, P. Li, S. Bi, X. H. Zhang, S. M. Chen, W. Peng, *Sens. Actuators, B* **2019**, *301*, 127136.
[47] X. Lin, Y. Fang, L. Zhu, J. Zhang, G. Huang, J. Wang, Y. Mei, *Adv. Opt. Mater.* **2016**, *4*, 936.
[48] J. I. Avila, R. J. Matelon, R. Trabol, M. Favre, D. Lederman, U. G. Volkmann, A. L. Cabrera, *J. Appl. Phys.* **2010**, *107*, 023504.
[49] V. P. Minkovich, A. B. Sotsky, A. V. Shilov, L. I. Sotskaya, *J. Appl. Spectrosc.* **2019**, *86*, 112.
[50] T. Zhan, C. Xu, F. Zhao, Z. Xiong, X. Hu, G. Huang, Y. Mei, J. Zi, *Appl. Phys. Lett.* **2011**, *99*, 211104.
[51] F. Zhao, T. Zhan, G. Huang, Y. Mei, X. Hu, *Lab Chip* **2012**, *12*, 3798.
[52] Z. Zhao, Z. Zhang, Y. Zhao, J. Liu, C. Liu, Z. Wang, G. Zheng, G. Huang, Y. Mei, *Adv. Funct. Mater.* **2019**, *29*, 1906365.
[53] Z. Zhao, Y. Kong, X. Lin, C. Liu, J. Liu, Y. He, L. Yang, G. Huang, Y. Mei, *J. Mater.Chem. A* **2020**, *8*, 26119.
[54] J. Ward, Y. Yang, F. Lei, X. Yun, S. Chormaic, *Optica* **2018**, *5*, 674.
[55] S. Tang, Y. Fang, Z. Liu, L. Zhou, Y. Mei, *Lab Chip* **2016**, *16*, 182.
[56] L. Ma, S. Li, V. Quinones, L. Yang, W. Xi, M. Jorgensen, S. Baunack, Y. Mei, S. Kiravittaya, O. Schmidt, *Adv. Mater.* **2013**, *25*, 2357.